MiR-142 Is Required for *Staphylococcus aureus* Clearance at Skin Wound Sites via Small GTPase-Mediated Regulation of the Neutrophil Actin Cytoskeleton

Katsuya Tanaka[1,2], Sang Eun Kim[1], Hiroki Yano[2], Gaku Matsumoto[1], Ryoma Ohuchida[1], Yuhoko Ishikura[1], Masatake Araki[3], Kimi Araki[3], Seongjoon Park[1], Toshimitsu Komatsu[1], Hiroko Hayashi[1], Kazuya Ikematsu[4], Katsumi Tanaka[2], Akiyoshi Hirano[2], Paul Martin[5], Isao Shimokawa[1] and Ryoichi Mori[1]

MicroRNAs (miRNAs) are small noncoding RNAs that regulate protein translation by binding to complementary target mRNAs. We previously identified two mature members of the *miR-142* family, *miR-142-5p* and *miR-142-3p*, as inflammation-related miRNAs with potential roles in wound healing. Here, we demonstrated that these two miRNAs are prominently expressed in wound-infiltrated neutrophils and macrophages and play central roles in wound healing. We generated *miR-142*$^{-/-}$ mice using the exchangeable gene-trap method and showed that healing of *Staphylococcus aureus*-infected skin wounds was significantly delayed in *miR-142*$^{-/-}$ mice compared with that in wild-type mice. *MiR-142*$^{-/-}$ mice exhibited abnormal abscess formation at *S. aureus*-infected skin wound sites and were also more susceptible to horizontal transmission of wound infections. *MiR-142*$^{-/-}$ neutrophils showed altered phagocytosis as a consequence of chemotactic behavior, including enhanced F-actin assembly, disturbed cell polarity, and increased cell motility. We showed that these changes were linked to cytoskeletal regulation, and that expression of the small GTPases was markedly increased in *miR-142*$^{-/-}$ neutrophils. Collectively, our data demonstrate that the *miR-142* family is indispensable for protection against *S. aureus* infection and its clearance at wound sites. *MiR-142-3p* and *miR-142-5p* play nonredundant roles in actin cytoskeleton regulation by controlling small GTPase translation in neutrophils at wound sites.

Journal of Investigative Dermatology (2017) **137,** 931–940; doi:10.1016/j.jid.2016.11.018

INTRODUCTION

Skin wound healing can be considered to consist of three phases: inflammation, proliferation/migration, and maturation/resolution. During the inflammatory phase, neutrophils are the first to migrate to the breach in the skin barrier to protect against microbes. Subsequently, during the proliferation/migration phase, macrophages are drawn to the wound where they secrete growth factors, cytokines, chemokines, and phagocytose-spent neutrophils, and other cell and matrix debris. In parallel, leading-edge epithelial cells are activated to re-cover the denuded wound surface, and local endothelial cells contribute to the sprouting of new blood vessels within the contractile granulation tissue. Finally, in the wound maturation/resolution phase, immune cells and contractile myofibroblasts resolve and/or die by apoptosis, and excess extracellular matrix is degraded by proteinase activity (Eming et al., 2014).

Staphylococcus aureus is an indigenous cutaneous bacterium frequently linked to the exacerbation of chronic skin wounds. Patients with diabetes and obese or immunosuppressed individuals are particularly at risk of nonhealing wounds accompanied by abnormal inflammatory responses, and associated with *S. aureus* overgrowth at such wound sites (Jenkins et al., 2016).

MicroRNAs (miRNAs) are key indirect regulators of protein translation, with each miRNA being able to target a broad range of up to hundreds of mRNAs (Baek et al., 2008; Selbach et al., 2008). It is becoming clear that miRNAs play critical roles in numerous physiological processes via their capacity to globally regulate the levels of large numbers of proteins within a cell, and hence their

[1]Department of Pathology, Nagasaki University School of Medicine and Graduate School of Biomedical Sciences, Sakamoto, Nagasaki, Japan; [2]Department of Plastic and Reconstructive Surgery, Nagasaki University School of Medicine and Graduate School of Biomedical Sciences, Sakamoto, Nagasaki, Japan; [3]Institute of Resource Development and Analysis, Kumamoto University, Honjo, Kumamoto, Japan; [4]Department of Forensic Pathology and Science, Nagasaki University School of Medicine and Graduate School of Biomedical Sciences, Sakamoto, Nagasaki, Japan; and [5]Schools of Biochemistry and Physiology, Pharmacology and Neuroscience, Faculty of Biomedical Sciences, University of Bristol, University Walk, Bristol, UK

Correspondence: Ryoichi Mori, Department of Pathology, Nagasaki University School of Medicine and Graduate School of Biomedical Sciences, 1-12-4 Sakamoto, Nagasaki 852-8523, Japan. E-mail: ryoichi@nagasaki-u.ac.jp

Abbreviations: CFU, colony-forming units; EGFP, enhanced green fluorescent protein; fMLP, N-formylmethionyl-leucyl-phenylalanine; lys, lysozyme M; miRNA, microRNA; 3′-UTR, 3′-untranslated region; WT, wild-type

Received 4 August 2016; revised 14 November 2016; accepted 16 November 2016; accepted manuscript published online 25 November 2016; corrected proof published online 14 February 2017

functional analysis in complex scenarios is becoming increasingly important (Lodish et al., 2008; Schwanhausser et al., 2011).

We identified the *miR-142* family members *miR-142-3p* and *miR-142-5p* as inflammation-related miRNAs with potential roles in wound healing by next-generation sequencing analysis and comparison between wild-type (WT) and *PU.1*-deficient (*PU.1*$^{-/-}$) mice, which lack inflammatory cells (neutrophils, macrophages, mast cells, and lymphocytes) and exhibit significantly faster and scar-free skin wound healing compared with WT mice (Martin et al., 2003). To test the potential function of skin wound healing, we generated *miR-142*$^{-/-}$ mice and reported that the healing of *S. aureus*-infected skin wounds was significantly delayed in comparison with that in WT mice. *MiR-142*$^{-/-}$ mice exhibited abnormal abscess formation at sites of *S. aureus*-infected skin wounds and were considerably more susceptible to horizontal transmission of wound infections. At the cell level, *miR-142*$^{-/-}$ neutrophils showed impairments of both chemotactic and phagocytic behavior, due to abnormal expression of *Rac* and *Rho* family of small GTPases and consequently disturbed F-actin assembly. Collectively, our data suggest a mechanistic link between *miR-142* family regulation of small GTPase levels and activity, and that these miRNAs function in the protection against *S. aureus* infection and its clearance at wound sites.

RESULTS AND DISCUSSION

MiR-142 contributes to the clearance of *S. aureus* at skin wound sites

We found that WT mice show comparatively high expression of *miR-142* family members in lung, spleen, colon, bone marrow, and thymus, suggesting that they play critical roles in immune defense (Supplementary Figure S1 online). To clarify the role of *miR-142* family members in skin wound healing, we examined their expression in wound-associated cells. We made wounds on the dorsal skin of WT mice, excised the wound tissue 1 and 3 days later, and isolated wound-infiltrated Ly-6G^{+} neutrophils and CD11b^{+} cells, which by immunoaffinity selection appeared to be up to 88% positive for the murine macrophage marker F4/80 (Austyn and Gordon, 1981). Quantitative PCR of the isolated cells confirmed that the wound-infiltrated neutrophils and macrophages indeed expressed *miR-142-3p* and *miR-142-5p* (Figure 1a). To examine the biological function of these miRNAs in skin wound healing, we generated whole-body *miR-142*$^{-/-}$ mice using an exchangeable gene-trap clone: Ayu21-KBW111 (http://egtc.jp/action/access/clone_detail?id=21-KBW111) (Araki et al., 2014) (Supplementary Figure S2 online). Our *miR-142*$^{-/-}$ mice had a phenotype similar to that of another *miR-142*$^{-/-}$ mouse strain, and exhibited splenomegaly, altered lymphocyte and red blood cell counts, and altered ratios of immune cells in the spleen (Supplementary Figure S3 and Supplementary Table S1 online) (Chapnik et al., 2014; Kramer et al., 2015).

Our initial studies of aseptic healing after streptozotocin-induced type 1 diabetes showed no significant difference between WT and *miR-142*$^{-/-}$ mice (Supplementary Figure S4 online). To determine whether the *miR-142* family is involved in wound repair and in the clearance of *S. aureus* infection in skin wounds, we made 4-mm excisional wounds in the dorsal skin of WT and *miR-142*$^{-/-}$ mice (Figure 1b), inoculated the wounds with *S. aureus* (1×10^8 colony-forming units [CFU]/10 μl), and monitored wound healing over the next several days (Figure 1c and d). In WT mice, the *S. aureus*-infected wound had not healed by 7 days after injury, but showed signs of healing between 7 and 14 days, with 90% of all wounds fully closed by 14 days. Healing of infected wounds was considerably worsened in *miR-142*$^{-/-}$ mice with wounds only just beginning to heal after 10 days and only 69% of wounds healed at 14 days. Histologic analysis allowed us to quantify the extent of re-epithelialization at various points during repair. Re-epithelialization at *S. aureus*-infected wound sites of *miR-142*$^{-/-}$ mice (0.62 ± 0.42 mm) was markedly slower than for *S. aureus*-infected wound sites of WT mice (1.0 ± 0.30 mm) (Figure 1e–g), but by 21 days, *S. aureus*-infected wound sites of both WT and *miR-142*$^{-/-}$ mice were fully closed. We assessed the quantity of live *S. aureus* at the wound sites and found that 6.2-fold more bacteria were present in the wounds of *miR-142*$^{-/-}$ mice (3.6×10^6 CFU/ml) compared with those of WT mice (5.8×10^5 CFU/ml) at 3 days after injury (Figure 1h), suggesting that neutrophilic clearance of infection might be the mechanistic link to poor wound closure.

In general, bacterial infections are driven by close contact (horizontal infection) (Fritz et al., 2012). We therefore next investigated the role of *miR-142* in the defense against naturally transmitted *S. aureus* skin infection. We established a horizontal infection model in which WT and *miR-142*$^{-/-}$ mice with aseptic skin wounds were housed in the same cage as a WT mouse with an *S. aureus*-infected skin wound (Figure 1i). We confirmed that wound-inoculated *S. aureus* bioparticles of the host mouse had been transmitted to two aseptic mice after 1 day (Figure 1j). We next assessed live *S. aureus* colonization and found significantly more (13.6-fold) *S. aureus* at the wound sites of *miR-142*$^{-/-}$ mice ($7.1 \times 10^5 \pm 7.0 \times 10^5$ CFU/ml) than at those of WT mice ($5.2 \times 10^4 \pm 4.0 \times 10^4$ CFU/ml) after 3 days (Figure 1k). We could not detect *S. aureus* colonization in the intact skin of WT and *miR-142*$^{-/-}$ mice. Collectively, our data show that *miR-142* participates in protection against *S. aureus* infection at skin wound sites.

MiR-142$^{-/-}$ mice show altered abscess formation and delayed immune cell phagocytosis at *S. aureus*-infected skin wound sites

Neutrophils are the first cells to migrate to skin wound sites (Eming et al., 2014) and are required for *S. aureus* clearance (van Kessel et al., 2014). To examine the spatiotemporal recruitment of neutrophils to *S. aureus*-infected wound sites in vivo, we crossed *miR-142*$^{-/-}$ mice to lysozyme M (*lys*)-enhanced green fluorescent protein (EGFP) mice, in which EGFP is knocked into the *lys* locus and is therefore specifically expressed in neutrophils and can be used as a neutrophil reporter at skin wound sites (Faust et al., 2000; Kim et al., 2008). In vivo imaging analysis of WT:*lys*-EGFP mice revealed that significantly more (2.16-fold) neutrophils (as measured by EGFP fluorescence intensity) are recruited to the sites of *S. aureus*-infected wounds than to aseptic wounds at 1 day after injury, but the recruitment of neutrophils to

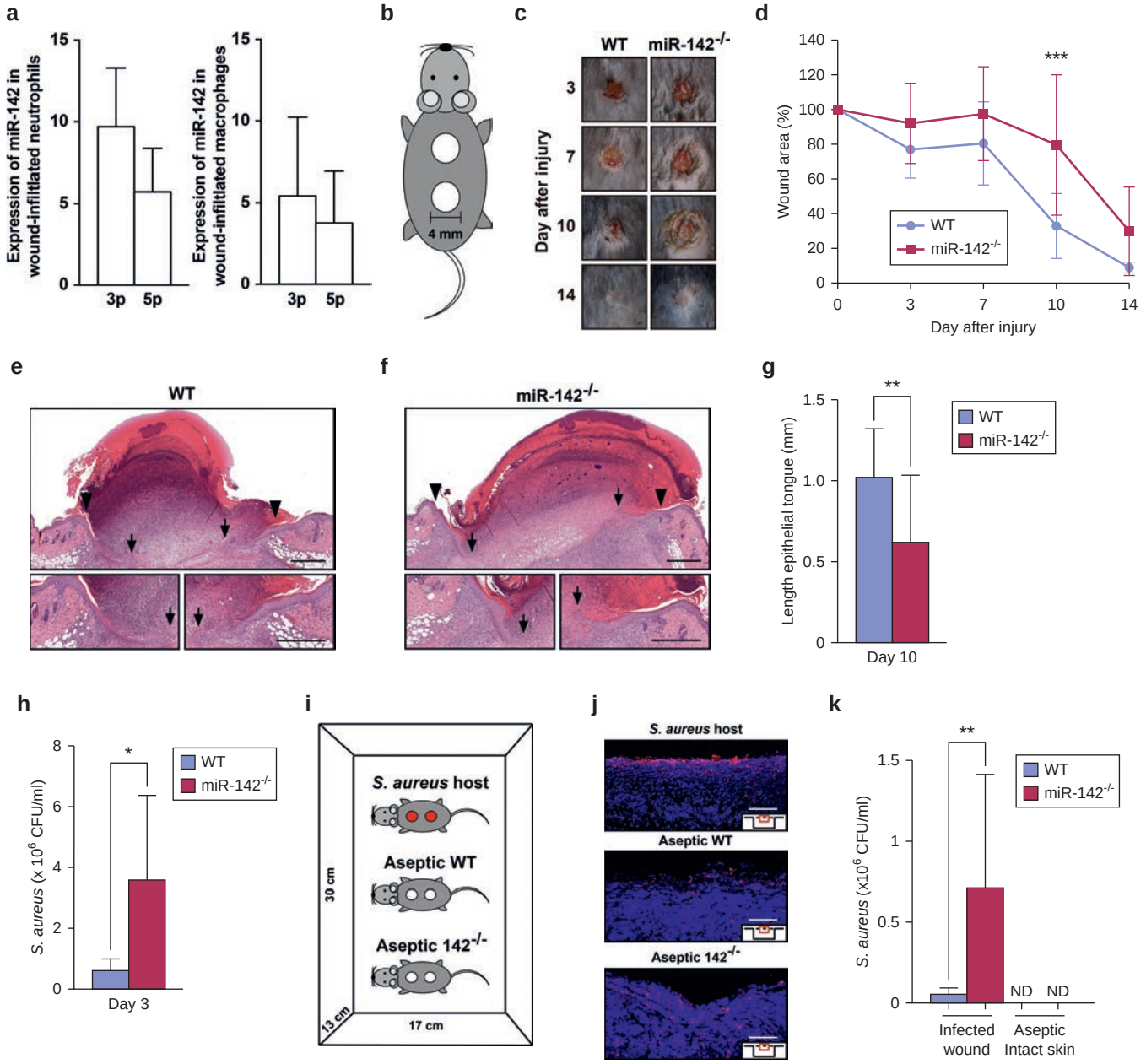

Figure 1. *MiR-142* is necessary for healing of *S. aureus*-infected skin wounds. (**a**) Expression of *miR-142* family members in wound-infiltrated neutrophils and macrophages, measured by qPCR (n = 3). (**b**) Schematic diagram of the murine skin wound healing model. Excisional wounds (4 mm thickness) were made in the shaved dorsal skin of adult male mice, and *S. aureus* was inoculated (1×10^8 CFU/10 μl) directly into the wound sites after injury. (**c**) Representative images of the gross appearance of *S. aureus*-infected excisional wounds in WT and *miR-142*$^{-/-}$ mice. (**d**) Time course showing the proportion of wounds remaining open compared with the initial wound area (WT, n = 10; *miR-142*$^{-/-}$, n = 14). (**e** and **f**) H&E staining of re-epithelialization in WT (**e**) and *miR-142*$^{-/-}$ mice (**f**) (wound margin [arrowheads] and the leading edge of epithelia [arrows]). (**g**) Measurement of epithelial tongue 10 days after injury (n = 12). (**h**) Quantity of colonizing *S. aureus* 3 days after injury, showing significantly higher levels at the wound sites of *miR-142*$^{-/-}$ mice (n = 6) compared with WT mice (n = 8). (**i**) Illustration of the horizontal infection study. WT and *miR-142*$^{-/-}$ mice with aseptic skin wounds were placed in the same cage as the host WT mouse bearing an *S. aureus*-infected wound. (**j**) Inoculated *S. aureus* (red) was naturally transmitted to other wound sites through direct contact. Nuclei were counterstained with DAPI. (**k**) Quantity of colonizing *S. aureus* was significantly higher at the wound sites of *miR-142*$^{-/-}$ than at those of WT mice 3 days after cohousing with the *S. aureus*-infected host mouse (n = 7). ND, not detected. All data are expressed as the mean ± SD. $^*P < 0.05$, $^{**}P < 0.01$, $^{***}P < 0.001$ by two-way analysis of variance (**d**), unpaired *t*-test (**g**) with Welch's test (**h, k**). CFU, colony-forming units; H&E, hematoxylin and eosin; qPCR, Quantitative PCR; SD, standard deviation; WT, wild type.

wounds is 1.65-fold lower in infected *miR-142*$^{-/-}$:*lys*-EGFP mice than in WT:*lys*-EGFP mice (Figure 2a and b).

A hallmark of *S. aureus* infection is abscess formation at the skin wound site, which involves neutrophils "walling off" the site of infection to enable effective bacterial clearance (Kobayashi et al., 2015; Molne et al., 2000). Histologic analysis of cross sections of WT wound tissues 3 days after injury showed abscesses with clearly recognizable borders under the dermis (Figure 2c). However, there was no clear abscess border in the wounds from *miR-142*$^{-/-}$ mice, but

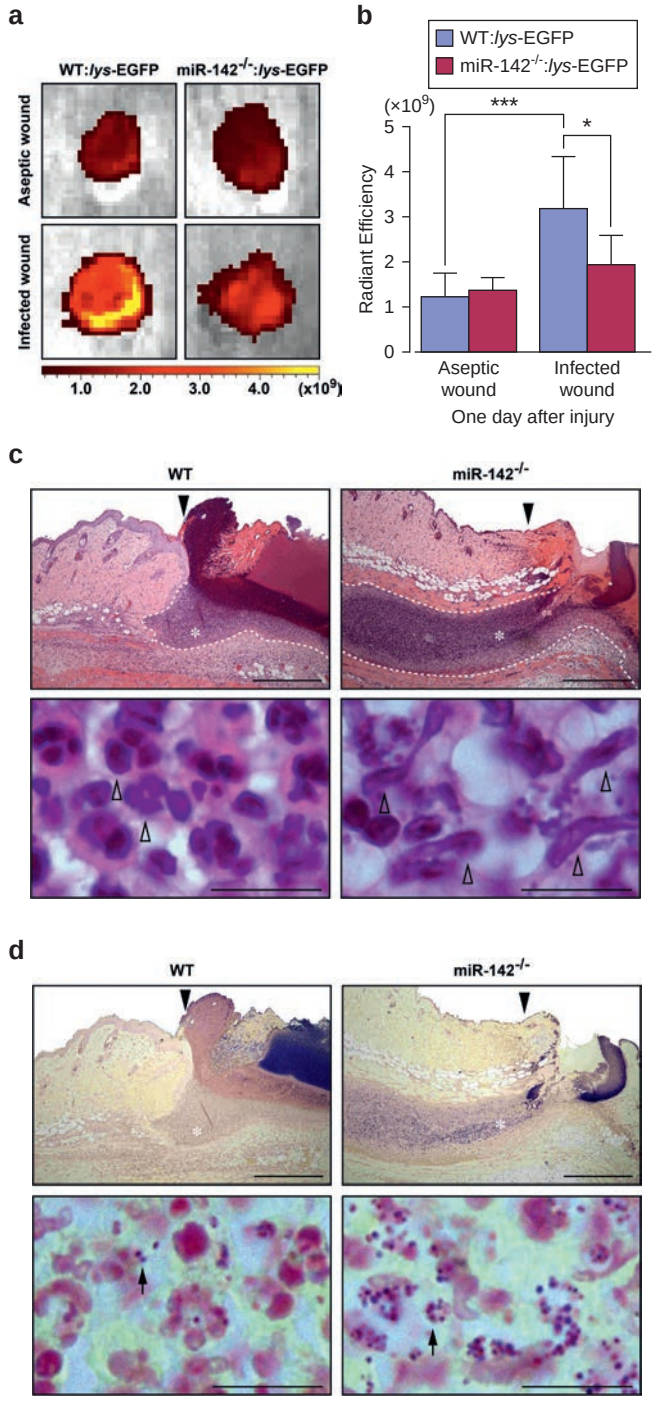

Figure 2. *MiR-142* is necessary for abscess formation and phagocytosis at the sites of *S. aureus*-infected skin wounds. (**a**) Representative in vivo fluorescence microscopy images of EGFP-expressing neutrophils at *S. aureus*-infected skin wound sites. Activity fluorescent imaging on a color scale overlaid on a gray scale image of wound sites. (**b**) Recruitment of neutrophils at *S. aureus*-infected skin wound sites, as measured by in vivo fluorescence. Values are the mean radiant efficiency ([p/s/cm^2/sr]/[μW/cm^2]) ± SD (aseptic model, n = 6; infection model, n = 8). (**c**) H&E staining shows altered abscess formation and cytomorphology of neutrophils at the wound sites of *miR-142*$^{-/-}$ mice 3 days after injury. The dotted line indicates the abscess interface. High-magnification view of the white asterisks indicates the recruitment of neutrophils (open arrowheads). Closed arrowheads indicate wound margin. (**d**) Images of Gram staining were obtained using serial sections. High-magnification view of the white asterisks indicates *S. aureus* (arrows). Images shown are representative of eight independent experiments (**c, d**). Scale bars = 500 μm (**c** and **d**, low magnification), 10 μm (**c** and **d**, high magnification). All data are expressed as the mean ± SD. *$P < 0.05$, ***$P < 0.001$ by one-way analysis of variance followed by Tukey's test. EGFP, enhanced green fluorescent protein; H&E, hematoxylin and eosin; lys, lysozyme M; SD, standard deviation; WT, wild type.

rather the abscess area had expanded beyond the wound area under the intact skin. Intriguingly, wound-infiltrated neutrophils in *miR-142*$^{-/-}$ mice exhibited a hyper-stretched morphology. Gram staining revealed the apparent abundance of *S. aureus* in *miR-142*$^{-/-}$ mice compared with that in WT mice (Figure 2d). Overall, 8% of WT mice (1/12 mice) and 50% of *miR-142*$^{-/-}$ mice (6/12 mice) retained an abscess at the wound site 10 days after injury.

We next measured phagocytic activity at the wound sites in vivo (Jones et al., 2013). For this, the wounds were inoculated with fluorescent *S. aureus* particles that do not become fluorescent until they are within a phagosome and then can be detected as punctate foci by confocal microscopy, allowing the extent of phagocytosis to be quantified. We found that the number of phagosomes at the wound sites of *miR-142*$^{-/-}$ mice was significantly lower than that at the wounds of WT mice (Figure 3a and b), indicating that *miR-142*$^{-/-}$ mice might exhibit abnormally low levels of phagocytosis.

To confirm that *miR-142* plays a functional role in leukocyte *S. aureus* attachment/engulfment at an early stage of infection in vivo, we harvested *S. aureus*-infected skin from wound sites at day 1 after injury, and performed transmission electron microscopy, which allowed us to observe the extracellular and subcellular localization of *S. aureus* in wound-infiltrated neutrophils at wound sites and intracellular vacuolar compartments (Kobayashi et al., 2010). *S. aureus* was found in clearly defined membrane-enclosed vacuoles in WT and *miR-142*$^{-/-}$ mice, indicating that *miR-142* is not absolutely essential for phagosome synthesis (Figure 3c). We determined the number of *S. aureus* within phagosomes and found that this number in *miR-142*$^{-/-}$ neutrophils was significantly reduced (mean value, 5 *S. aureus*/neutrophil) when compared with that in WT neutrophils (mean value, 12 *S. aureus*/neutrophil) (Figure 3d). These results indicate that *miR-142* in neutrophils could at least contribute to the process of *S. aureus* clearance until engulfment.

We next measured the time course of phagocytosis of bacteria by bone marrow-derived neutrophils in vitro. The proportion of phagosome-positive WT neutrophils gradually increased for 10 minutes after coculture of these cells with fluorescent *S. aureus* bioparticles (Figure 3e). In contrast, *miR-142*$^{-/-}$ neutrophils were largely still not phagosome-positive at 30 minutes and beyond. Taken together, these results indicate that *miR-142* may play a critical role in neutrophil clearance of *S. aureus* infection during skin wound healing.

MiR-142 regulates neutrophil polarity and uropod retraction during chemotaxis

The morphology of *miR-142*$^{-/-}$ neutrophils appeared similar to that of neutrophils in zebrafish deficient in *miR-142ab*, in which these cells fail to developmentally disperse, suggesting that the migratory capacity of *miR-142* in mammalian neutrophils might also be altered (Fan et al., 2014). To investigate

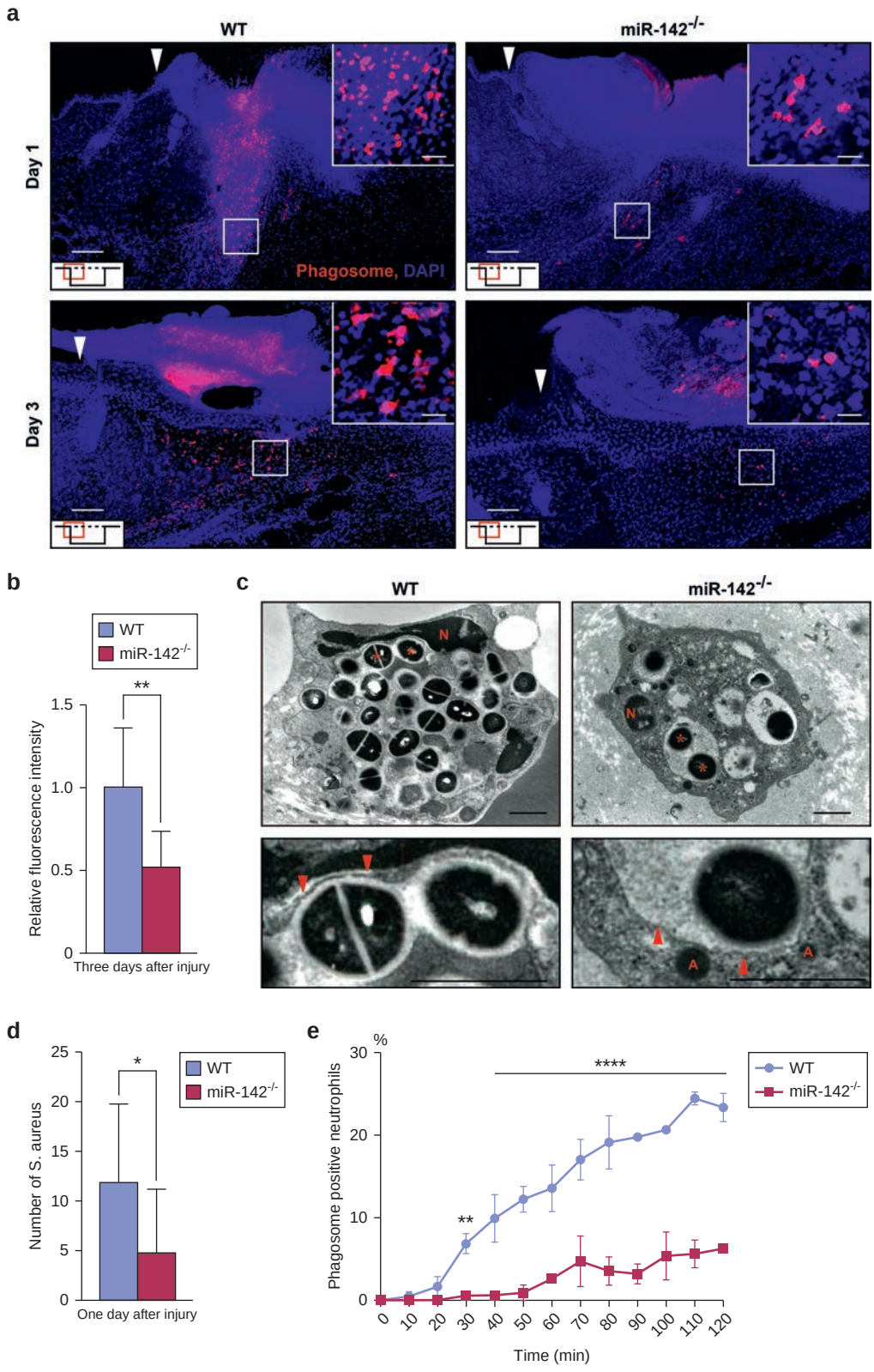

Figure 3. *MiR-142* is necessary for phagocytosis at the sites of *S. aureus*-infected skin wounds. (**a**) Representative images showing that the number of phagosomes (red) at the wound sites was lower in *miR-142*$^{-/-}$ mice than in WT mice. High-magnification view of the boxed areas (inset). Nuclei were counterstained with DAPI (blue). Arrowheads indicate the wound margin. (**b**) Fluorescence intensity analysis of phagosome (WT; n = 11, *miR-142*$^{-/-}$; n = 9). (**c**) TEM images of neutrophils from wound sites 1 day after injury. Top panels: *S. aureus* phagocytosis of *miR-142*$^{-/-}$ neutrophils was markedly attenuated. Asterisks indicate *S. aureus*. N, nucleus. Bottom panels: *S. aureus* was found in clearly defined membrane-enclosed vacuoles in WT and *miR-142*$^{-/-}$ mice. Arrowheads indicate intact phagosomes/phagosome membranes. A, azurophil granule. Images shown are representative of two independent experiments. (**d**) Number of *S. aureus* within phagosomes in neutrophils in *miR-142*$^{-/-}$ mice (18 cells from 3 mice) was significantly decreased compared with that in WT neutrophils (12 cells from 3 mice). (**e**) Time course showing reduced phagocytosis of bone marrow-derived neutrophils from *miR-142*$^{-/-}$ mice compared with cells derived from WT mice (124 cells from 2 WT mice, 92 cells from 3 *miR-142*$^{-/-}$ mice). Scale bars = 100 μm (**a**), 20 μm (**a**, inset), 1 μm (**c**). All data are expressed as the mean ± SD. $*P < 0.05$, $**P < 0.01$, $****P < 0.0001$ by unpaired *t*-test (**b**) with Welch's test (**d**) and two-way analysis of variance followed by Bonferroni's test (**e**). SD, standard deviation; TEM, transmission electron microscopy; WT, wild type.

the mechanisms of neutrophil chemotaxis, we incubated bone marrow-derived neutrophils in the presence of a local source of the chemotactic peptide N-formylmethionyl-leucyl-phenylalanine (fMLP) and imaged their migratory tracks by differential interference contrast imaging microscopy. fMLP-stimulated *miR-142*$^{-/-}$ neutrophils exhibited multiple leading edges and a hyper-stretched morphology (reminiscent of that seen in vivo in *miR-142*$^{-/-}$ mice, as mentioned above), as they migrated toward the attractant (Figure 4a, Supplementary Movies S1 and S2 online). To structurally and

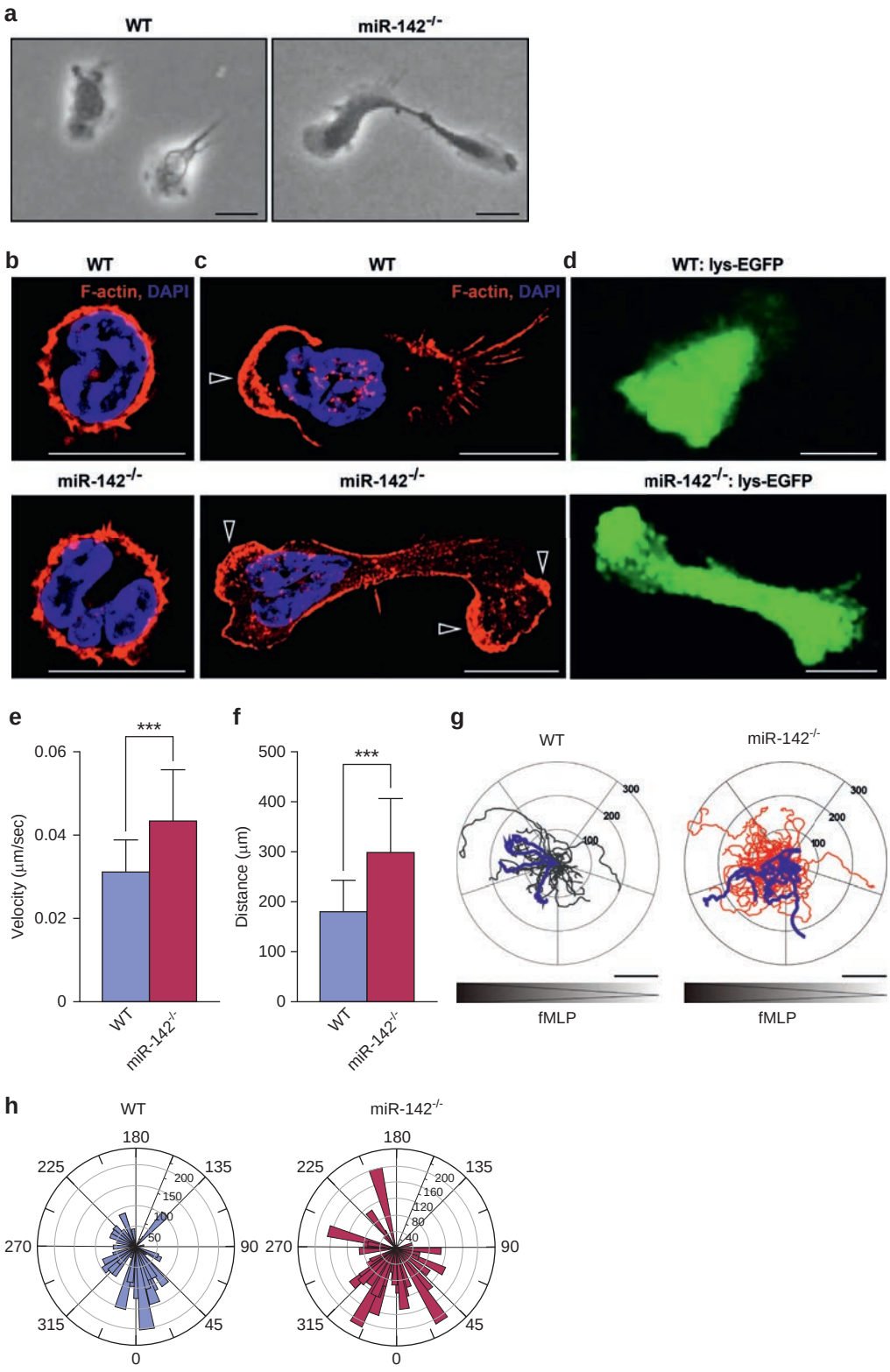

Figure 4. *MiR-142*$^{-/-}$ neutrophils display abnormal migration. (**a**) Representative differential interference contrast images showing abnormal cytomorphology of *miR-142*$^{-/-}$ neutrophils during fMLP-stimulated chemotaxis. Related to Supplementary Movies S1 (WT neutrophils) and S2 (*miR-142*$^{-/-}$ neutrophils). (**b**) Representative SIM images showing normal morphology of unstimulated WT and *miR-142* neutrophils (F-actin, red; DAPI, blue). (**c**) Representative SIM images of *miR-142*$^{-/-}$ neutrophil chemotaxis 30 minutes after the addition of fMLP. Dense F-actin staining is observed at the sides of the lamellipodia. (**d**) Cytomorphological changes in *miR-142*$^{-/-}$:*lys*-EGFP neutrophils after fMLP stimulation. Related to Supplementary Movies S3 (WT:*lys*-EGFP neutrophils) and S4 (*miR-142*$^{-/-}$:*lys*-EGFP neutrophils). (**e** and **f**) Quantification of the velocity of (**e**) and total migrating distance covered by (**f**) fMLP-stimulated WT:*lys*-EGFP and *miR-142*$^{-/-}$:*lys*-EGFP neutrophils (43 cells from 3 WT and *miR-142*$^{-/-}$ mice). (**g**) Tracking of fMLP-stimulated WT:*lys*-EGFP and *miR-142*$^{-/-}$:*lys*-EGFP neutrophils (n = 43). Blue lines indicate four representative neutrophils. Note that the direction of fMLP-stimulated movement of *miR-142*$^{-/-}$:*lys*-EGFP neutrophils is markedly different from that of WT:*lys*-EGFP neutrophils. (**h**) Angular graph shows no preferential migration directionality relationship between WT and *miR-142*$^{-/-}$ neutrophils. Band and length of band indicates one cell and direction that is from start point to end point. Scale bars = 10 μm (**a**–**d**). All data are expressed as the mean ± SD. ***$P < 0.001$ by unpaired *t*-test with Welch's test (**e, f**). EGFP, enhanced green fluorescent protein; fMLP, N-formylmethionyl-leucyl-phenylalanine; lys, lysozyme M; SD, standard deviation; SIM, structured illumination microscopy; WT, wild type.

functionally characterize the neutrophils during chemotaxis, we examined the F-actin network in cells stained with fluorescent phalloidin using structured illumination microscopy, a form of super-resolution fluorescence microscopy (Cox, 2015). Before stimulation, WT and *miR-142*$^{-/-}$ neutrophils had identical morphologies (Figure 4b); however, on fMLP stimulation, *miR-142*$^{-/-}$ neutrophils exhibited markedly increased F-actin content within their lamellipodia (Figure 4c), as well as clear uropod retraction defects (Supplementary Figure S5 online). We visualized chemotaxis of WT:*lys*-EGFP and *miR-142*$^{-/-}$:*lys*-EGFP neutrophils by confocal microscopy and confirmed that fMLP-stimulated

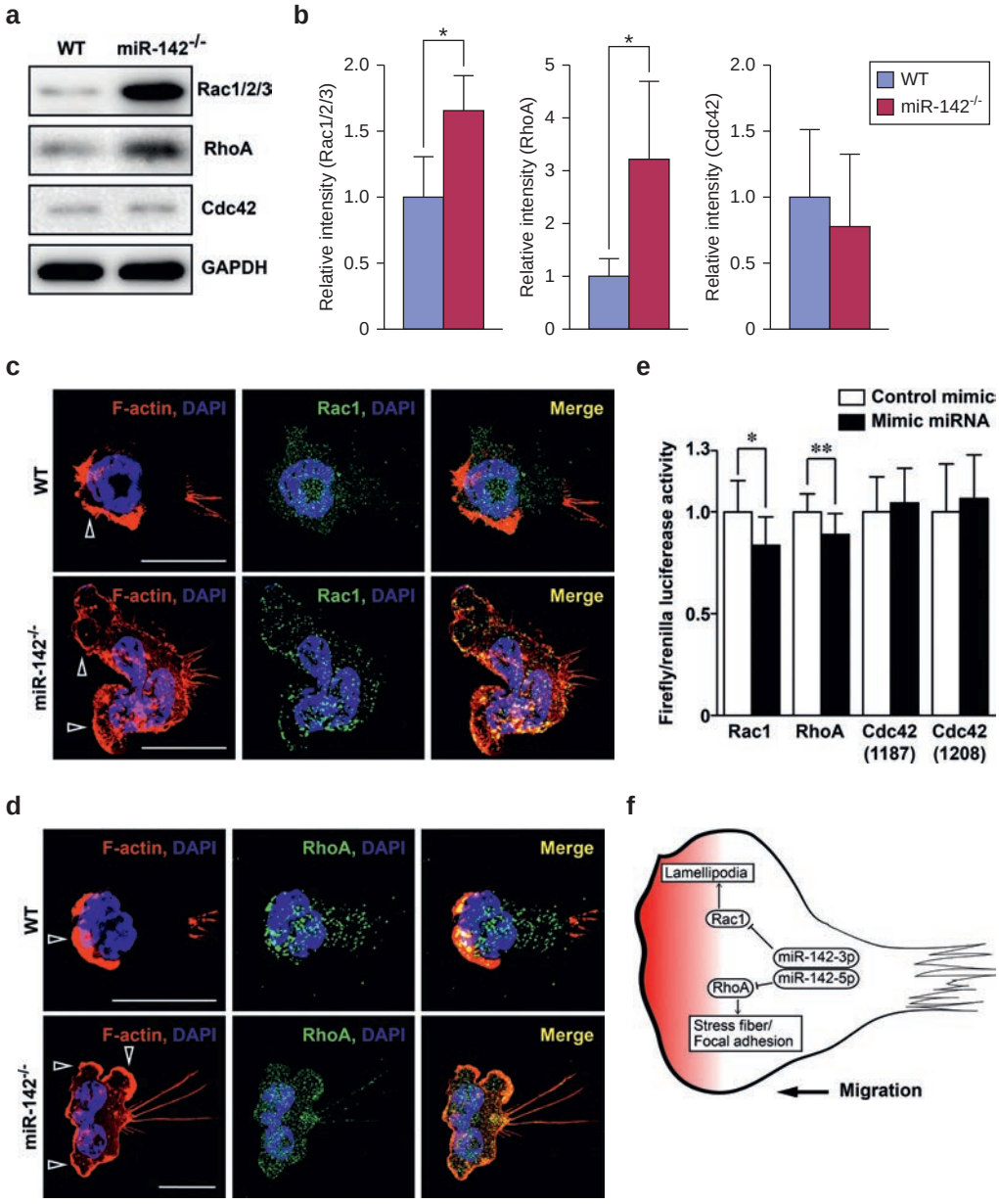

Figure 5. *MiR-142* family regulates translation of small GTPases during chemotaxis. (**a**) Immunoblot analysis of *Rac1*, *RhoA*, and *Cdc42* expression in neutrophils 30 minutes after fMLP stimulation. (**b**) Densitometric analysis of *Rac1*, *RhoA*, and *Cdc42* expression (n = 4). (**c** and **d**) Representative SIM images showing the expression and localization of *Rac1* and *RhoA* in neutrophils 30 minutes after fMLP stimulation of chemotaxis. A marked difference is observed between WT and *miR-142*$^{-/-}$ neutrophils. Scale bar = 10 μm. (**e**) *MiR-142-3p* and *miR-142-5p* bind with high affinity to *Rac1* and *RhoA* 3′-UTRs, respectively, but not to the *Cdc42* 3′-UTR. A luciferase reporter vector encoding the 3′-UTRs was cotransfected with *miR-142* mimics into 3T3 cells. A decrease in luciferase activity indicates binding of the miRNA mimic to the 3′-UTR of the target sequence. (**f**) Proposed model for the regulation of cytoskeleton organization in neutrophils by the *miR-142* family. *MiR-142-3p* and *miR-142-5p* control lamellipodia and stress fiber/focal adhesion via *Rac1* and *RhoA* protein synthesis. Rupture of *miR-142* function leads to abnormal morphology and chemotaxis. All data are expressed as the mean ± SD. $^{*}P < 0.05$ and $^{**}P < 0.01$ by the unpaired *t*-test (**b, e**). fMLP, N-formylmethionyl-leucyl-phenylalanine; GAPDH, glyceraldehyde-3-phosphate dehydrogenase; miRNA, microRNA; SD, standard deviation; SIM, structured illumination microscopy; 3′-UTRs, 3′-untranslated region; WT, wild type.

miR-142$^{-/-}$:*lys*-EGFP neutrophils behaved similarly to *miR-142*$^{-/-}$ neutrophils (Figure 4d, Supplementary Movies S3 and S4 online). Time-lapse videos of 2-hour duration revealed that *miR-142*$^{-/-}$:*lys*-EGFP neutrophils moved toward a high concentration of fMLP at a higher velocity than WT:*lys*-EGFP neutrophils (Figure 4e and f). The fMLP-stimulated movement of *miR-142*$^{-/-}$:*lys*-EGFP neutrophils was also significantly more sustained than that of WT:*lys*-EGFP neutrophils (WT 82.5 ± 4.7 minutes [43 cells from 3 mice]; *miR-142*$^{-/-}$ 105.0 ± 4.2 minutes [47 cells from 3 mice], $P = 0.0006$; Supplementary Movies S3 and S4). However, *miR-142*$^{-/-}$:*lys*-EGFP neutrophils tended to lose their polarity more rapidly than WT cells, leading to a haphazard migratory route (Figure 4g), even though preferential migration directionality in *miR-142*$^{-/-}$:*lys*-EGFP neutrophils (22 per 47 cells with a higher frequency of migration in the direction of 0° ± 45°) was not significantly different from that in WT:*lys*-EGFP neutrophils (21 per 46 cells with a higher frequency of migration in the direction of 0° ± 45°) (Figure 4h). In general, neutrophils migrate toward a wound or site of infection and then remain static while secreting biomolecules at the site of inflammation. We speculate that *miR-142*$^{-/-}$ neutrophils may have defective "stop signaling," which normally allows them to shift from the migratory phase to the cytokine secretory phase, resulting in a greater susceptibility of *miR-142*$^{-/-}$ mice to infection at wound sites. Taken together, our data indicate that *miR-142* in neutrophils contributes to the maintenance of polarity and the shift from the migratory to the static, bactericidal state.

Expression of small GTPases is regulated by *miR-142* in neutrophils

The small GTPases *Rho*, *Rac*, and *Cdc42* are necessary for various aspects of leukocyte migration induced by

chemotactic cues during the innate immune response (Bokoch, 2005), and mouse genome informatics (see Supplementary Materials and Methods online) predicts that all three of these molecular switches may be candidate target genes for *miR-142* (Supplementary Figure S6 online). Indeed, *miR-142-3p* knockdown enhances the migration of human $CD4^+$ T cells and modulates actin cytoskeleton regulation through *Rac1* and *Rock2*, which are *miR-142-3p* target genes (Liu et al., 2014). Our related previous in vivo imaging studies of small GTPases in *Drosophila* embryo wound inflammation showed that *Rac*, *Cdc42*, and *Rho* signaling contributes to immune cell lamellipodial activity, migratory polarity, and uropod retraction, respectively, as these cells migrate to wound sites (Stramer et al., 2005). Here, we show that the expression of *Rho* and *Rac*, but not *Cdc42*, was significantly increased and their localization was altered in fMLP-stimulated *miR-142*$^{-/-}$ neutrophils, compared with those in WT neutrophils, as measured by immunoblotting and immunocytochemistry (Figure 5a–d). To investigate the direct mechanism behind this, we tested whether the *miR-142* family can bind to mammalian *Cdc42*, *Rac1*, and *RhoA* target 3′-untranslated region (3′-UTR) mRNAs. Specifically, we cotransfected the murine fibroblast cell line with *miR-142-3p* or *miR-142-5p* mimics with a firefly luciferase vector encoding the 3′-UTRs of the predicted mRNA target sites (Supplementary Figure S6). Analysis of luciferase activity showed that the *miR-142-3p* and *miR-142-5p* mimics bound to *Rac1* and *RhoA* 3′-UTRs, respectively (Figure 5e). These results suggest that *miR-142-3p* and *miR-142-5p* interact with *Rac1* and *RhoA* mRNA 3′-UTRs, respectively, which may in part influence neutrophil chemotaxis (Figure 5f).

Chapnik et al. (2014) reported that megakaryocytes from *miR-142*$^{-/-}$ mice exhibit disturbed actin cytoskeletal dynamics owing to changes in the expression levels of several cytoskeletal regulatory genes, such as cofilin-2 (*Cfl2*), Rho GTPase activating protein 35 (*Arhgap35*), and Wiskott-Aldrich syndrome-like (*Wasl*), all of which are target genes for *miR-142-3p*. Taken together with our results, this suggests that the *miR-142* family might play a role in regulating neutrophil migration by modulating *Rac* and *Rho* expression levels and the consequent regulation of the actin cytoskeleton, which is clearly pivotal for efficient neutrophil migration.

We found that the *miR-142* family may regulate the expression of small GTPases and thus orchestrate neutrophil motility during chemotaxis, but it is known that the small GTPase family also plays a central role in phagocytosis. For instance, Fc receptor-mediated phagocytosis, which depends on binding to the Fc portion of antibodies, is mediated by *Cdc42* and *Rac*, and the internalization of complement-opsonized particles is dependent on *Rho* (Caron and Hall, 1998). Our findings in this study reveal that *miR-142* may be involved in neutrophil migration through effects on small GTPase expression, and we speculate that it may also control engulfment efficiency. Macrophage, lymphocyte, and cytokine production are important for bacterial killing (Hume et al., 2006). We are currently investigating the molecular mechanism linking *miR-142* and other biological functions (i.e., cytokine production) in detail.

Several hereditary diseases that involve genes critical for neutrophil function or production have been identified, some of which are associated with immunodeficiency and severe susceptibility to bacterial infection; for example, using a zebrafish model of wound repair and systemic infection, we revealed that immunodeficiency-related Wiskott-Aldrich syndrome protein (*WASp*), which is known to coordinate actin polymerization, plays an essential role in leukocyte wound recruitment and *S. aureus* clearance (Jones et al., 2013). A number of studies have shown that *Rac* isoforms are crucially important for neutrophil functions in mice, such as chemotaxis, bacterial killing, and nicotinamide adenine dinucleotide phosphate oxidase pathway activation (Koh et al., 2005; Pick, 2014), and genetic defects in small GTPase family members also affect neutrophil function in humans; for example, neutrophils derived from individuals with a point mutation in *Rac2* exhibit decreased chemotactic polarization, azurophilic granule secretion, and superoxide anion production (Williams et al., 2000). Although *miR-142* deficiencies have not yet been identified in humans, our findings implicate *miR-142* family members in disorders related to neutrophil function and immunodeficiency.

In conclusion, we have revealed that the *miR-142* family regulates actin cytoskeleton dynamics in neutrophils by controlling small GTPase translation, and showed that it plays a central role in the protection against *S. aureus* infection at skin wound sites. Our findings suggest that these miRNAs might be involved in multiple regulatory steps that enable the killing of opportunistic pathogens at wound sites.

MATERIALS AND METHODS

Skin wounding

All experiments were conducted according to the provisions of the Ethics Review Committee for Animal Experimentation at Nagasaki University. The wound model was established as described previously (Mori et al., 2014). In brief, full-thickness excisional wounds (4-mm biopsy punch; Kai Industries, Seki, Japan) were made in the dorsal skin (after shaving under anesthesia) of 6- to 12-week-old mice (Figure 1b). Wound tissues were harvested using a 6-mm biopsy punch (Kai Industries). The gross appearance of wound closure was recorded using a digital camera. Wound areas were calculated using Photoshop CS4 (Adobe Systems, San Jose, CA).

Artificial and horizontal *S. aureus* infection at skin wound sites

S. aureus type strain (NBRC 100910) was obtained from the National Institute of Technology and Evaluation (Tokyo, Japan). Mice were inoculated with *S. aureus* (1×10^8 CFU/10 μl) at the skin wound sites. The presence of *S. aureus* at the wound sites was quantified by two methods. *S. aureus* gene-specific PCR was performed with a Quick Primer *S. aureus* kit (Takara Bio, Kusatsu, Japan) and an ABI PRISM 7900HT Sequence Detection System (Applied Biosystems, Foster, CA). Alternatively, bacteria were quantified by counting CFU after culture.

For the horizontal *S. aureus* infection study, two WT mice and one *miR-142*$^{-/-}$ mouse were placed overnight in a cage (17 cm in length, 30 cm in width, and 13 cm in height) to check that they did not fight each other. The next day, skin wounds were made on all three mice and the wound site of one WT mouse was inoculated with Alexa Fluor 594-conjugated *S. aureus* BioParticles (10 μl of 20 mg/ml; Life Technologies, Carlsbad, CA) or *S. aureus*

(1×10^8 CFU/10 μl). The second WT mouse and the *miR-142*$^{-/-}$ mouse were placed in the same cage as the host mouse for 3 days. The amount of *S. aureus* at the wound sites was then quantified by CFU counting.

Analysis of phagocytosis at wound sites

pHrodo Red *S. aureus* Bioparticles (10 μl of 10 mg/ml; Life Technologies) were inoculated into the skin wounds. After excision, tissues were fixed in 4% paraformaldehyde, embedded in O.C.T. Compound, and frozen. Sections (60 μm thick) were counterstained with DAPI. Phagosomes were visualized by z-stack confocal fluorescence microscopy (C2+ system; Nikon Corporation, Tokyo, Japan) equipped with Plan Apo VC20x (0.75 NA), and the images were processed using IMARIS software (Bitplane, Zurich, Switzerland).

Analysis of phagocytosis in vitro

Ly-6G$^+$ neutrophils were isolated from bone marrow by MACS Separation (Miltenyi Biotec GmbH, Bergisch Gladbach, Germany), in accordance with the manufacturer's instructions. The phagocytosis assay was performed with pHrodo Red *S. aureus* Bioparticles. In brief, 30 μl of pHrodo Red *S. aureus* Bioparticles (1 mg/ml) were mixed with neutrophils suspended in Dulbecco's modified Eagle's medium without phenol red (1×10^5 cells/200 μl) and placed in a glass-bottomed dish. Cells were incubated in an atmosphere of 5% CO_2 at 37°C in a stage top incubator (Tokai Hit, Fujinomiya, Japan). Cells were examined by confocal microscopy (C2+ system; Nikon Corporation) equipped with Plan Apo VC20x (0.75 NA). Images were acquired every minute and fluorescent phagosome-positive cells were counted every 10 minutes.

Statistical analysis

Data are presented as the mean ± standard deviation. Differences between means were analyzed with GraphPad Prism 6 software (GraphPad Software, San Diego, CA).

SUPPLEMENTARY MATERIALS AND METHODS

The generation of *miR-142*$^{-/-}$ mice and *miR-142*$^{-/-}$:*lys*-EGFP mice; isolation of tissue neutrophils, macrophages, T lymphocytes, and B lymphocytes; establishment of the streptozotocin-induced diabetes model; and methods for miRNA isolation and quantitative PCR analysis, histology, transmission electron microscopy, chemotaxis assay, immunocytochemistry, total protein extraction and immunoblotting, and assay for miRNA binding to the 3′-UTR of mRNA are described in the Supplementary Materials and Methods.

CONFLICT OF INTEREST

The authors state no conflict of interest.

ACKNOWLEDGMENTS

We thank Drs Thomas Graf (Centre for Genomic Regulation, Barcelona, Spain), Shintaro Hashimoto, and Masaki Honda (Kumamoto University, Kumamoto, Japan) for providing *lys*-EGFP mice. We are also grateful for comments on the experiments and manuscript from Dr Eun Seong Hwang (University of Seoul, Seoul, South Korea), for assistance with the transmission electron microscopy analysis from Takashi Suematsu (Department of Electron Microscopy, Nagasaki University). This work was supported in part by the Ministry of Education, Culture, Sports, Science and Technology of Japan (Grant-in-Aid for Research Activity Start-up, 20890258; Grants-in-Aid for Young Scientists A, 21689049 and 24689069; Grant-in-Aid for Scientific Research B, 16H05493; Challenging Exploratory Research, 23650484 and 25560055 to RM and 26670773 to HY; Grants-in-Aid for Young Scientists B, 26861503 and 16K20361 to KT); Takeda Science Foundation (RM); the Uehara Memorial Foundation (RM); the Nakatomi Foundation (RM); the Wellcome Trust (Senior Investigator Award 097791MA, PM); and the Royal Society (International Joint Projects, PM and RM).

SUPPLEMENTARY MATERIAL

Supplementary material is linked to the online version of the paper at www.jidonline.org, and at http://dx.doi.org/10.1016/j.jid.2016.11.018.

REFERENCES

Araki M, Nakahara M, Muta M, Itou M, Yanai C, Yamazoe F, et al. Database for exchangeable gene trap clones: pathway and gene ontology analysis of exchangeable gene trap clone mouse lines. Dev Growth Differ 2014;56:161–74.

Austyn JM, Gordon S. F4/80, a monoclonal antibody directed specifically against the mouse macrophage. Eur J Immunol 1981;11:805–15.

Baek D, Villen J, Shin C, Camargo FD, Gygi SP, Bartel DP. The impact of microRNAs on protein output. Nature 2008;455:64–71.

Bokoch GM. Regulation of innate immunity by Rho GTPases. Trends Cell Biol 2005;15:163–71.

Caron E, Hall A. Identification of two distinct mechanisms of phagocytosis controlled by different Rho GTPases. Science 1998;282:1717–21.

Chapnik E, Rivkin N, Mildner A, Beck G, Pasvolsky R, Metzl-Raz E, et al. miR-142 orchestrates a network of actin cytoskeleton regulators during megakaryopoiesis. Elife 2014;3:e01964.

Cox S. Super-resolution imaging in live cells. Dev Biol 2015;401:175–81.

Eming SA, Martin P, Tomic-Canic M. Wound repair and regeneration: mechanisms, signaling, and translation. Sci Transl Med 2014;6:265sr6.

Fan HB, Liu YJ, Wang L, Du TT, Dong M, Gao L, et al. miR-142-3p acts as an essential modulator of neutrophil development in zebrafish. Blood 2014;124:1320–30.

Faust N, Varas F, Kelly LM, Heck S, Graf T. Insertion of enhanced green fluorescent protein into the lysozyme gene creates mice with green fluorescent granulocytes and macrophages. Blood 2000;96:719–26.

Fritz SA, Hogan PG, Hayek G, Eisenstein KA, Rodriguez M, Krauss M, et al. *Staphylococcus aureus* colonization in children with community-associated *Staphylococcus aureus* skin infections and their household contacts. Arch Pediatr Adolesc Med 2012;166:551–7.

Hume EB, Cole N, Garthwaite LL, Khan S, Willcox MD. A protective role for IL-6 in staphylococcal microbial keratitis. Invest Ophthalmol Vis Sci 2006;47:4926–30.

Jenkins TC, Knepper BC, McCollister BD, Moore SJ, Pawlowski SW, Perlman DM, et al. Failure of outpatient antibiotics among patients hospitalized for acute bacterial skin infections: what is the clinical relevance? Am J Emerg Med 2016;34:957–62.

Jones RA, Feng Y, Worth AJ, Thrasher AJ, Burns SO, Martin P. Modelling of human Wiskott-Aldrich syndrome protein mutants in zebrafish larvae using in vivo live imaging. J Cell Sci 2013;126(Pt 18):4077–84.

Kim MH, Liu W, Borjesson DL, Curry FR, Miller LS, Cheung AL, et al. Dynamics of neutrophil infiltration during cutaneous wound healing and infection using fluorescence imaging. J Invest Dermatol 2008;128:1812–20.

Kobayashi SD, Braughton KR, Palazzolo-Ballance AM, Kennedy AD, Sampaio E, Kristosturyan E, et al. Rapid neutrophil destruction following phagocytosis of *Staphylococcus aureus*. J Innate Immun 2010;2:560–75.

Kobayashi SD, Malachowa N, DeLeo FR. Pathogenesis of *Staphylococcus aureus* abscesses. Am J Pathol 2015;185:1518–27.

Koh AL, Sun CX, Zhu F, Glogauer M. The role of Rac1 and Rac2 in bacterial killing. Cell Immunol 2005;235:92–7.

Kramer NJ, Wang WL, Reyes EY, Kumar B, Chen CC, Ramakrishna C, et al. Altered lymphopoiesis and immunodeficiency in miR-142 null mice. Blood 2015;125:3720–30.

Liu J, Li W, Wang S, Wu Y, Li Z, Wang W, et al. MiR-142-3p attenuates the migration of CD4(+) T cells through regulating actin cytoskeleton via RAC1 and ROCK2 in arteriosclerosis obliterans. PloS One 2014;9:e95514.

Lodish HF, Zhou B, Liu G, Chen CZ. Micromanagement of the immune system by microRNAs. Nat Rev Immunol 2008;8:120–30.

Martin P, D'Souza D, Martin J, Grose R, Cooper L, Maki R, et al. Wound healing in the PU.1 null mouse—tissue repair is not dependent on inflammatory cells. Curr Biol 2003;13:1122–8.

Molne L, Verdrengh M, Tarkowski A. Role of neutrophil leukocytes in cutaneous infection caused by *Staphylococcus aureus*. Infect Immun 2000;68:6162–7.

Mori R, Tanaka K, de Kerckhove M, Okamoto M, Kashiyama K, Kim S, et al. Reduced FOXO1 expression accelerates skin wound healing and attenuates scarring. Am J Pathol 2014;184:2465–79.

Pick E. Role of the Rho GTPase Rac in the activation of the phagocyte NADPH oxidase: outsourcing a key task. Small GTPases 2014;5:e27952.

Schwanhausser B, Busse D, Li N, Dittmar G, Schuchhardt J, Wolf J, et al. Global quantification of mammalian gene expression control. Nature 2011;473:337–42.

Selbach M, Schwanhausser B, Thierfelder N, Fang Z, Khanin R, Rajewsky N. Widespread changes in protein synthesis induced by microRNAs. Nature 2008;455:58–63.

Stramer B, Wood W, Galko MJ, Redd MJ, Jacinto A, Parkhurst SM, et al. Live imaging of wound inflammation in Drosophila embryos reveals key roles for small GTPases during in vivo cell migration. J Cell Biol 2005;168:567–73.

van Kessel KP, Bestebroer J, van Strijp JA. Neutrophil-mediated phagocytosis of *Staphylococcus aureus*. Front Immunol 2014;5:467.

Williams DA, Tao W, Yang F, Kim C, Gu Y, Mansfield P, et al. Dominant negative mutation of the hematopoietic-specific Rho GTPase, Rac2, is associated with a human phagocyte immunodeficiency. Blood 2000;96:1646–54.